

UC Davis

UC Davis Previously Published Works

Title

Fast sulfate formation from oxidation of SO₂ by NO₂ and HONO observed in Beijing haze

Permalink

<https://escholarship.org/uc/item/8vv6583j>

Journal

Nature Communications, 11(1)

ISSN

2041-1723

Authors

Wang, Junfeng

Li, Jingyi

Ye, Jianhuai

et al.

Publication Date










2020

DOI

10.1038/s41467-020-16683-x

Peer reviewed

Fast sulfate formation from oxidation of SO₂ by NO₂ and HONO observed in Beijing haze

Junfeng Wang ^{1,2,12}, Jingyi Li ^{1,12}, Jianhuai Ye ^{2,12}, Jian Zhao³, Yangzhou Wu^{1,4}, Jianlin Hu¹, Dantong Liu⁴, Dongyang Nie^{1,5}, Fuzhen Shen¹, Xiangpeng Huang¹, Dan Dan Huang⁶, Dongsheng Ji³, Xu Sun⁷, Weiqi Xu³, Jianping Guo⁸, Shaojie Song², Yiming Qin², Pengfei Liu ², Jay R. Turner⁹, Hyun Chul Lee ¹⁰, Sungwoo Hwang¹⁰, Hong Liao ¹, Scot T. Martin ², Qi Zhang¹¹, Mindong Chen¹, Yele Sun³, Xinlei Ge ¹✉ & Daniel J. Jacob ²✉

Severe events of wintertime particulate air pollution in Beijing (winter haze) are associated with high relative humidity (RH) and fast production of particulate sulfate from the oxidation of sulfur dioxide (SO₂) emitted by coal combustion. There has been considerable debate regarding the mechanism for SO₂ oxidation. Here we show evidence from field observations of a haze event that rapid oxidation of SO₂ by nitrogen dioxide (NO₂) and nitrous acid (HONO) takes place, the latter producing nitrous oxide (N₂O). Sulfate shifts to larger particle sizes during the event, indicative of fog/cloud processing. Fog and cloud readily form under winter haze conditions, leading to high liquid water contents with high pH (>5.5) from elevated ammonia. Such conditions enable fast aqueous-phase oxidation of SO₂ by NO₂, producing HONO which can in turn oxidize SO₂ to yield N₂O. This mechanism could provide an explanation for sulfate formation under some winter haze conditions.

¹ Jiangsu Key Laboratory of Atmospheric Environment Monitoring and Pollution Control, School of Environmental Science and Engineering, Nanjing University of Information Science and Technology, Nanjing 210044, China. ² John A. Paulson School of Engineering and Applied Sciences, Harvard University, Cambridge, MA 02138, USA. ³ State Key Laboratory of Atmospheric Boundary Layer Physics and Atmospheric Chemistry, Institute of Atmospheric Physics, Chinese Academy of Sciences, Beijing 100029, China. ⁴ Department of Atmospheric Sciences, School of Earth Sciences, Zhejiang University, Hangzhou 310027, China. ⁵ School of Atmospheric Sciences, Nanjing University, Nanjing 210023, China. ⁶ State Environmental Protection Key Laboratory of Formation and Prevention of Urban Air Pollution Complex, Shanghai Academy of Environmental Sciences, Shanghai 200233, China. ⁷ State Key Laboratory of Urban and Regional Ecology Research Center for Eco-Environmental Sciences, Chinese Academy of Sciences, Beijing 100085, China. ⁸ State Key Laboratory of Severe Weather, Chinese Academy of Meteorological Sciences, Beijing 100081, China. ⁹ Department of Energy, Environmental and Chemical Engineering, Washington University in Saint Louis, St. Louis, MO 63130, USA. ¹⁰ Samsung Advanced Institute of Technology, Suwon-si, Gyeonggi-do 16678, Republic of Korea. ¹¹ Department of Environmental Toxicology, University of California Davis, Davis, CA 95616, USA. ¹² These authors contributed equally: Junfeng Wang, Jingyi Li, Jianhuai Ye. ✉email: caxinra@163.com; djacob@fas.harvard.edu

Beijing experiences severe air pollution events in winter, commonly called winter haze. The concentration of fine particulate matter with aerodynamic diameter less than or equal to $2.5\ \mu\text{m}$ ($\text{PM}_{2.5}$) can exceed $200\ \mu\text{g m}^{-3}$ on a 24-h average basis during these events¹, considerably higher than the 24-h Chinese National Ambient Air Quality Standard of $75\ \mu\text{g m}^{-3}$. Winter haze events are often associated with high relative humidity (RH)^{2–5} and a major contribution of sulfate to total $\text{PM}_{2.5}$ ⁶. Sulfate is produced in the atmosphere by oxidation of sulfur dioxide (SO_2) emitted from coal combustion^{7,8}. But the photochemical oxidants known to drive atmospheric oxidation of SO_2 (hydroxyl radical, hydrogen peroxide, ozone) have very low concentrations under typical winter haze conditions^{9,10}. This has led to considerable debate regarding the mechanisms responsible for sulfate formation in winter haze^{9,11–13}.

The high-RH conditions characteristic of winter haze cause particulate matter to take up water, enabling aqueous-phase pathways for SO_2 oxidation. SO_2 is a weak acid with moderate water solubility (Henry's law constant $K_H = 1.2\ \text{M atm}^{-1}$ at 298 K) that dissociates in water to form bisulfite (HSO_3^- ; $pK_{a,1} = 1.9$ at 298 K) and sulfite (SO_3^{2-} ; $pK_{a,2} = 7.2$ at 298 K). Bisulfite and sulfite are converted to sulfate by a number of aqueous-phase oxidants with rates dependent on pH¹⁴. As the air cools at night or through rising motions the haze can turn to fog and low clouds (RH > 100%), increasing the atmospheric liquid water content (LWC) by orders of magnitude and hence the importance of SO_2 aqueous-phase oxidation pathways.

Most previous studies of sulfate formation during Beijing haze events have focused on mechanisms taking place in the ubiquitous haze particles (RH < 100%) rather than in the more sporadic fog and cloud (RH > 100%)^{13,15–17}. Haze particles are concentrated aqueous solutions with pH that can be estimated from standard thermodynamics¹⁸. Aqueous-phase oxidation of SO_2 by nitrogen dioxide (NO_2) in haze has been proposed^{9,11,13}, with NO_2 originating from vehicular emissions, but requires higher pH than the 4–5 range inferred from thermodynamic calculations^{19–21}. Some studies have suggested that oxidation by NO_2 would be enhanced by fog^{9,13,17}. Aqueous-phase autoxidation of SO_2 by molecular oxygen catalyzed by transition metal ions (TMI) has been proposed^{22,23} but is poorly constrained due to the lack of information on TMI concentration, complexation, and solubility²⁴. A recent study suggests that aqueous-phase oxidation by hydrogen peroxide (H_2O_2) in haze could be significant¹⁰. Yet another suggestion is that some of the reported sulfate could actually be hydroxymethanesulfonate (HMS) produced by in-cloud complexation of HSO_3^- and SO_3^{2-} with formaldehyde (HCHO)^{25,26}.

Here we present detailed chemical observations during a Beijing haze event in December 2016 where $\text{PM}_{2.5}$ concentrations reached $400\ \mu\text{g m}^{-3}$. We observe fast sulfate production as RH increases over the course of the event, leading to extensive nighttime fog and low clouds, and find a concurrent increase of nitrous oxide (N_2O). N_2O is a product of aqueous-phase SO_2 oxidation by dissolved nitrous acid (HONO)^{27–29}, and observations of HONO during the event support this sulfate formation mechanism. Most of the HONO appears in turn to be produced by aqueous-phase SO_2 oxidation by NO_2 , leading us to propose a two-step fog-enabled mechanism for sulfate formation during winter haze events.

Results

Field observations. Figure 1 shows the time series of selected variables measured at our field site on the rooftop of an Institute of Atmospheric Physics (IAP) building in urban Beijing during December 4–22, 2016. The start of the campaign on December

4 sampled the end of a haze event that terminated on December 5 with passage of a cold front. Variable conditions were observed during December 6–15 (data not shown). An extended haze event then developed over the December 16–22 period, with 24-h average $\text{PM}_{2.5}$ exceeding $200\ \mu\text{g m}^{-3}$ for 6 successive days before a cold front swept in with clean air on December 22.

Wind speed during the December 16–22 haze event was persistently low in the range of $0.3\text{--}1.5\ \text{m s}^{-1}$ and the mixed layer height (MLH) was less than 600 m above ground level (AGL), decreasing to 300 m at night. The early part of the event on December 16–19 (labeled Stage I in Fig. 1) had moderate RH in the 40–75% range. On December 20–21 (Stage II) the RH rose to above 75% as temperatures cooled to an average of 271 K at night, and dense nighttime fog with LWC as high as $0.5\ \text{g m}^{-3}$ was observed at the Beijing Observatory meteorological station 20 km to the south (Fig. 1). Beijing International Airport also reported fog during that period (Supplementary Fig. 1). Dense fog was not observed at our site, but the visibility dropped below a few hundred meters and low clouds formed just 50 m above ground (Supplementary Fig. 2).

$\text{PM}_{2.5}$ concentrations rose to over $400\ \mu\text{g m}^{-3}$ during the high-RH period (Stage II) in concert with a rise in sulfate, while nitrate remained at the same concentration as in Stage I ($47\ \mu\text{g m}^{-3}$). Black carbon (BC) increased from 9.4 to $13.1\ \mu\text{g m}^{-3}$. SO_2 concentrations were relatively high in Stage I but nearly depleted in Stage II, indicating rapid oxidation of emitted SO_2 to sulfate.

Figure 2 shows that the sulfate particles measured by high-resolution aerosol mass spectrometer (HR-AMS) shifted to larger sizes during Stage II while the organic particles did not, consistent with sulfate formation taking place in fog and low cloud (cloud-mediated coagulation would have affected both sulfate and organic particles). Mean $\text{PM}_{2.5}$ increased from $210\ \mu\text{g m}^{-3}$ in Stage I to $330\ \mu\text{g m}^{-3}$ in Stage II, while sulfate measured by HR-AMS increased fourfold from 10 to $40\ \mu\text{g m}^{-3}$. The sampling efficiency of the HR-AMS instrument (PM_{10}) drops off rapidly for particles above $1\text{-}\mu\text{m}$ diameter³⁰, implying that actual sulfate levels during Stage II were probably much higher than measured. Indeed, $\text{PM}_{2.5}$ sulfate concentrations measured at the site by on-line ion chromatography (URG-9000D Ambient Ion Monitor) were 1.5–2 times larger than the HR-AMS measurements during Stage II (Supplementary Fig. 3). Some of the sulfate particles could even be larger than $\text{PM}_{2.5}$ due to swelling at high RH.

Evidence for SO_2 oxidation by HONO. A remarkable feature of the observations in Stage II is the large rise in N_2O concentrations concurrently with sulfate. N_2O is a major greenhouse gas with a globally dominant biogenic source³¹. It is chemically inert in the troposphere. Vehicles and coal combustion may be a significant source of N_2O in Beijing³², but this would not explain the N_2O rise in Stage II because no parallel rise was observed for BC (Fig. 1).

Figure 3 shows the relationships between the concentrations of sulfate and different nitrogen oxide species (N_2O , HONO, NO_2 , and PM_{10} nitrate) observed in Stages I and II. The relationships are shown only for nighttime hours (19:00–06:00) to minimize strong common dependences on diurnal changes in mixed layer depth, and to avoid the effect of fast HONO photolysis in the daytime. Sulfate correlates positively with all species in Stage I, which may reflect common dependences on atmospheric mixing and ventilation. In Stage II, sulfate is positively correlated with N_2O (including a step increase) and with HONO, but negatively correlated with NO_2 and nitrate. This suggests a change in the regime for sulfate production in Stage II with associated production of N_2O . Looking back at the tail end of the previous haze event on December 4, which also featured high-RH

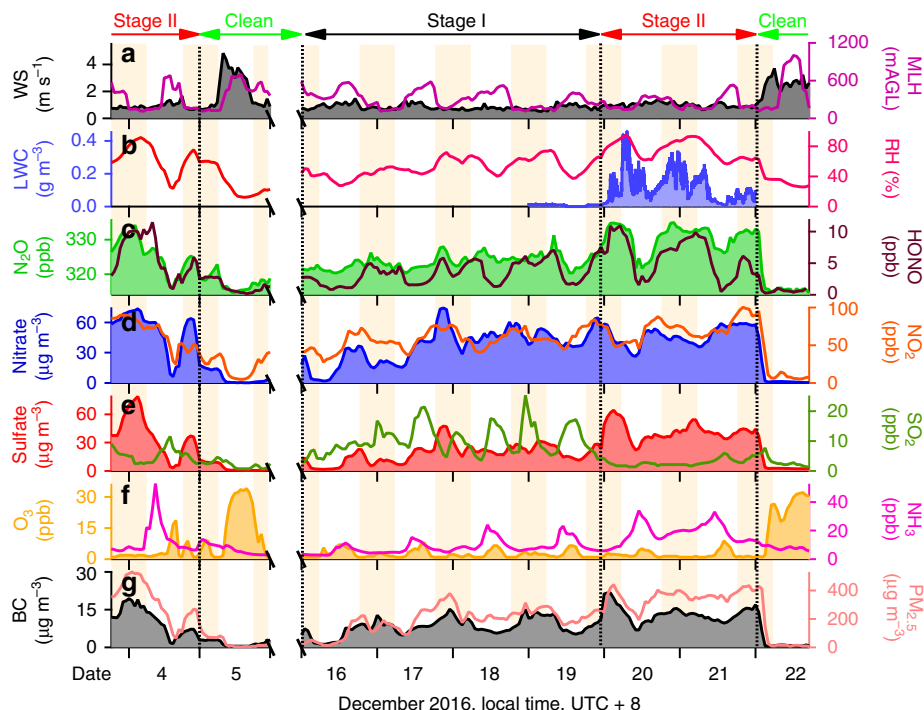


Fig. 1 Chronology of a winter haze event. The figure shows the time series of meteorological parameters and chemical species measured in Beijing on December 4–22, 2016. The measurements were made from the roof of an Institute of Atmospheric Physics (IAP) building except for liquid water content (LWC) measured at the Beijing Observatory of the China Meteorological Administration 20 km to the southeast, and PM_{2.5} concentration measured at the Beijing Olympic Center Observatory 4 km to the northeast. UTC+8 denotes Coordinated Universal Time + 8 h and represents local solar time in hours. **a** 10-m wind speed (WS) and mixing layer height (MLH) above ground level (AGL). **b** LWC and relative humidity (RH); **c** N₂O and HONO concentrations; **d** PM₁ nitrate and NO₂ concentrations; **e** PM₁ sulfate and SO₂ concentrations; **f** ozone (O₃) and ammonia (NH₃) concentrations; and **g** black carbon (BC) and PM_{2.5} concentrations. The campaign sampled the tail end of a haze event on December 4, terminated by passage of a cold front on December 5 and followed by variable conditions on December 6–15 (not shown, note break in time axis). It then sampled an extended pollution episode on December 16–22 with initially moderate RH of 40–75% (Stage I), followed by high RH (>75%) including dense nighttime fog at the Beijing Observatory (Stage II), and ending on December 22 with the passage of a cold front. Nighttime periods are shaded. Sulfate and nitrate measurements are from the HR-AMS instrument with a size cut of 1-μm diameter (see text).

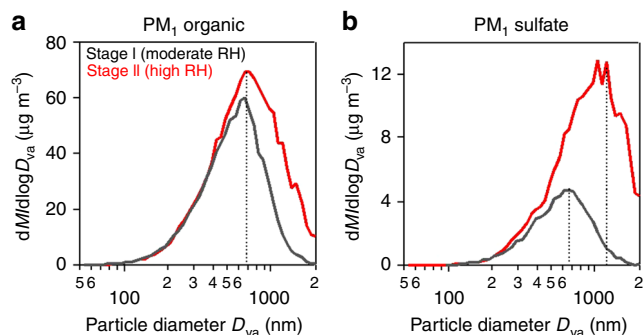
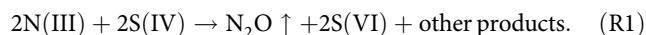


Fig. 2 Size distributions of organic and sulfate particles. The Figure shows mass-based size distributions of **(a)** organic and **(b)** sulfate particles in Stages I and II of the December 16–22, 2016 haze event. *M* denotes mass and *D_{va}* denotes particle vacuum aerodynamic diameter. The measurements were made by the HR-AMS instrument with 50% size cut at 1-μm diameter, hence the data are shown as PM₁ (particulate matter with less than 1-μm diameter). Mass modal diameters are shown as dotted lines.

conditions, we again see elevated N₂O together with sulfate (Fig. 1).

N₂O is a product of the aqueous-phase oxidation of SO₂ by HONO^{28,29}. HONO is moderately soluble in water (Henry’s law constant *K_H* = 49 M atm⁻¹ at 298 K) and dissociates as a weak acid (*pK_a* = 3.2 at 298 K) to increase its partitioning in the aqueous phase³³. The aqueous-phase oxidation of SO₂ by HONO

can be expressed stoichiometrically as follows^{28,29}:



Here N(III) ≡ HONO(aq) + NO₂⁻ denotes the dissolved HONO species, S(IV) ≡ SO₂·H₂O + HSO₃⁻ + SO₃²⁻ denotes the dissolved SO₂ species, and S(VI) ≡ H₂SO₄(aq) + HSO₄⁻ + SO₄²⁻ denotes the sulfate species. The other products may include H₂O or H⁺ depending on the speciation of N(III), S(IV), and S(VI). A laboratory study by Martin et al.²⁸ gives a rate expression for sulfate formation from reaction (R1) at pH < 4:

$$d[\text{S(VI)}]/dt = k_1[\text{H}^+]^{0.5}[\text{N(III)}][\text{S(IV)}], \quad (1)$$

where *k*₁ = 142 M^{-3/2} s⁻¹. Another study by Oblath et al.²⁷ gives a rate expression

$$d[\text{S(VI)}]/dt = k'_1[\text{H}^+][\text{N(III)}][\text{S(IV)}], \quad (2)$$

with *k*₁′ = 4800 M⁻² s⁻¹ for 3 < pH < 7. Even though these rate expressions show positive [H⁺] dependences, the rates actually increase with pH because both [S(IV)] and [N(III)] are inversely dependent on [H⁺] over the relevant pH range.

The increase of N₂O in Stage II concomitant with sulfate suggests that reaction (R1) could be a source of sulfate. However, the slopes of the sulfate–N₂O regression lines in Fig. 3 are similar for Stages I and II and not consistent with the 2:1 stoichiometry of reaction (R1). A possible explanation is that the PM₁ sulfate measurements underestimated total sulfate concentrations during Stage II, as shown above. In addition, it is likely that the correlations and slopes are mainly driven by mixing rather than

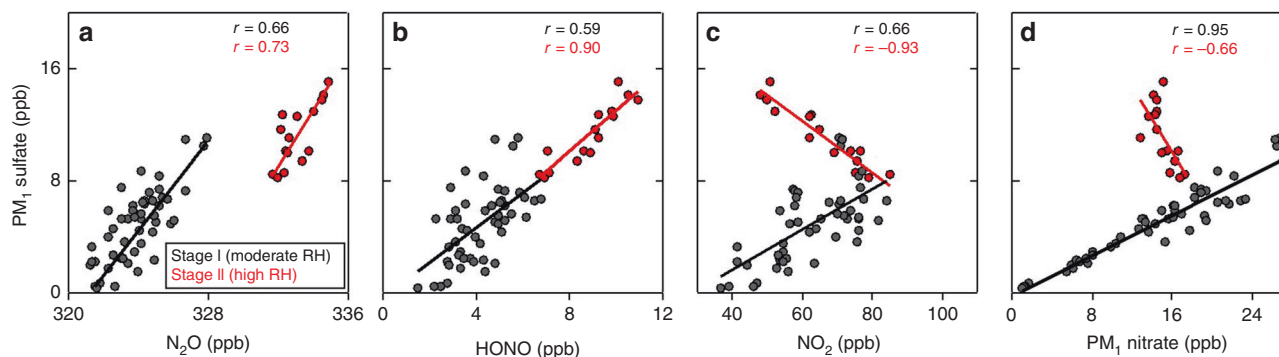


Fig. 3 Relationships between sulfate and nitrogen oxide concentrations. Data are shown for Stages I and II of the December 16–22, 2016 haze event. Concentrations of sulfate and nitrogen oxides are expressed in common parts per billion (ppb) units ($1\mu\text{g m}^{-3}$ sulfate = 0.23 ppb at $T = 273.15$ K). Individual points are hourly mean values from Fig. 1 during nighttime hours (19:00–6:00 local time). The figure shows scatterplots of PM₁ sulfate versus **a** nitrous oxide (N₂O); **b** nitrous acid (HONO); **c** nitrogen dioxide (NO₂); **d** PM₁ nitrate. Pearson correlation coefficients (r) and reduced-major-axis regression lines are shown separately for Stages I and II.

chemistry, as is frequently observed in polluted air masses^{34,35}. The signature of the reaction (R1) taking place in Stage II would then be manifested by the step increase in N₂O between the two Stages.

Importance of fog and cloud. Reaction (R1) requires fog or cloud to proceed at an appreciable rate. LWCs in haze are too low. It also requires a relatively high pH. The mean gaseous ammonia concentration observed during Stage II was 14 ppb (Fig. 1), typical of previous observations during haze events³⁶ and mainly attributable to emissions from fuel combustion³⁷. Fog has a much higher pH than haze under high-ammonia conditions because of efficient scavenging of ammonia at high LWC. Whereas ammonia volatility limits the pH of haze aqueous solutions to a 4–5 range even with ammonia in large excess^{19,20,38–40}, the corresponding pH range in fog is 6–7^{9,13,21,41,42}. Higher pH in haze can be achieved if dust is a significant component^{9,21,42} but low LWC is still a limitation. PM_{2.5} concentrations of dust cations (Ca²⁺, Mg²⁺) were low at our site, as described in the “Methods” section.

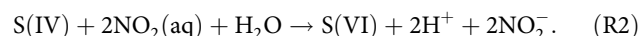
Our sampling site did not actually experience fog during Stage II, but the cloud deck extended down to 50 m (Supplementary Fig. 2), and surface air would have been processed by that low cloud and/or by fog elsewhere. We estimate a fog/cloud pH of 5.7 on the basis of our mean measured value of 14 ppb total ammonia to be partitioned into the fogwater; a fog LWC of 0.15 g m^{-3} ; sulfate, nitrate, and chloride PM_{2.5} present as their ammonium salts; and a temperature of 271 K (see “Methods”). Past observations for Beijing in winter indicate a fog/cloud pH range of 4.7–6.9^{7,11,26,43,44}. Sensitivity to pH will be examined in the “Discussion” section.

We can estimate the e-folding lifetime for SO₂ oxidation by HONO in nighttime fog on the basis of a fog with pH 5.7 and LWC of 0.15 g m^{-3} , and assuming a mean nighttime total HONO concentration of 9 ppb as measured during Stage II (Fig. 1). This involves applying the rate expression for reaction (R1) with Henry’s law and acid dissociation constants computed at 271 K (Supplementary Table 1). We find a fogwater nitrite (N(III), mainly as NO₂⁻) concentration of $2.2\mu\text{mol L}^{-1}$, which leads to an e-folding SO₂ lifetime of 3.8 h using the rate expression of Martin et al.²⁸ extended to pH 5.7 but 79 h using the rate expression of Oblath et al.²⁷. The former would imply a major role of HONO as SO₂ oxidant while the latter would imply an insignificant role. As we will see, the HONO concentration in fog could actually be much higher than measured at our site, which would increase the importance of reaction (R1). The observed

increase of N₂O in Stage II does suggest an important role for reaction (R1).

Evidence for SO₂ oxidation by NO₂ and production of HONO.

A remarkable result in Fig. 3 is the positive correlation of sulfate with HONO during Stage II, and the negative correlations with NO₂ and nitrate. Aqueous-phase loss of NO₂ during haze and fog is generally thought to be driven by particle-phase disproportionation to HONO and HNO₃¹¹, but if this were the case we would expect an increase in nitrate during Stage II in contrast to what was observed (Figs. 1 and 3). Aqueous-phase oxidation of S(IV) by NO₂ (aq) in fog is an alternative explanation for the depletion of NO₂ and produces both HONO and sulfate²⁸, which would be consistent with the positive correlation observed between the two (Fig. 3):



Laboratory studies give a rate expression for reaction (R2) as

$$d[\text{S(VI)}]/dt = k_2[\text{NO}_2(\text{aq})][\text{S(IV)}], \quad (3)$$

with $k_2 = 2 \times 10^6\text{ M}^{-1}\text{ s}^{-1}$ for the pH range 5.8–6.4 (Lee and Schwartz⁴⁵) and $k_2 = 1.2\text{--}1.5 \times 10^7\text{ M}^{-1}\text{ s}^{-1}$ for the pH range 5.3–6.8 (Clifton et al.⁴⁶). For a mean nighttime NO₂ concentration of 50 ppb during Stage II (Fig. 1), and a fog with LWC = 0.15 g m^{-3} and pH = 5.7, we find an SO₂ e-folding lifetime of 1–7 min against loss by reaction (R2) depending on which value of k_2 is used, sufficiently short in any case for SO₂ depletion. Reaction (R2) further produces N(III) as NO₂⁻, which in a fog of pH 5.7 would remain in the aqueous phase and may thus go on to oxidize SO₂ by reaction (R1). If reaction (R1) is sufficiently fast, following the rate expression of Martin et al.²⁸, then a steady state would be established at night between production of NO₂⁻ in the fog by reaction (R2) and loss by reaction (R1), resulting in an effective sulfate mass yield of 2 from reaction (R2).

An SO₂ oxidation mechanism in nighttime fog involving reaction (R2) followed by reaction (R1) would be consistent with our observed enhancement of N₂O. In that mechanism, one mole of N₂O is produced for every three moles of SO₂ oxidized. Starting from a SO₂ level of 20 ppb in Stage I (Fig. 1), complete oxidation of that SO₂ to sulfate would produce 7 ppb N₂O, consistent with the ≈ 5 ppb increase of N₂O observed between Stage I and Stage II (Fig. 3). The mechanism both produces and consumes HONO in the oxidation of SO₂, whereas N₂O is a terminal product, which may explain why HONO shows a positive correlation with sulfate in Stage II but not a step increase. One would similarly expect one mole of NO₂ to be consumed for

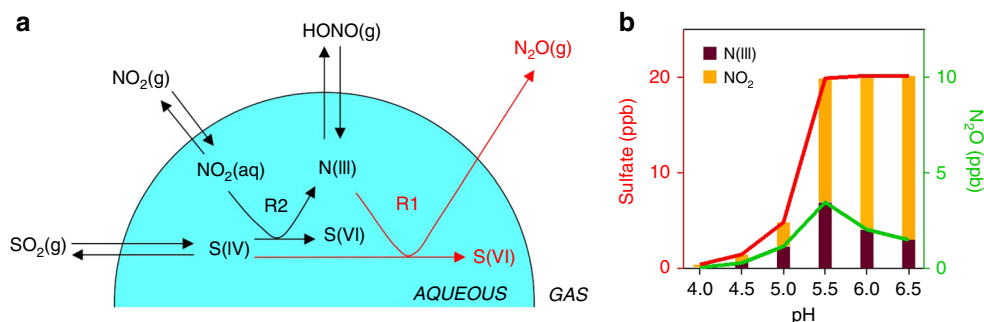


Fig. 4 **SO₂ oxidation mechanism.** **a** Illustration of the mechanism for SO₂ oxidation to sulfate by NO₂ and HONO in fog and cloud. Here S(IV) ≡ SO₂•H₂O + HSO₃⁻ + SO₃²⁻ denotes the different forms of dissolved SO₂, S(VI) ≡ H₂SO₄(aq) + HSO₄⁻ + SO₄²⁻ denotes the different forms of sulfate, and N(III) ≡ HNO₂(aq) + NO₂⁻ denotes the different forms of dissolved HONO. S(IV) is oxidized in the aqueous phase by dissolved NO₂ (reaction (R2)), producing N(III) which may oxidize additional S(IV) and produce N₂O by reaction (R1). **b** pH-dependent sulfate and N₂O production from the (R2) + (R1) mechanism. The plot shows accumulated concentrations of sulfate and N₂O after 5 h in a nighttime fog air parcel simulation initialized with [SO₂] = 20 ppb, [NO₂] = 80 ppb, and [HONO] = 5 ppb, with a fog LWC = 0.15 g m⁻³ and T = 271 K. Contributions from aqueous-phase SO₂ oxidation by HONO (reaction (R1)) and NO₂ (reaction (R2)) are shown separately. A sulfate production of 20 ppb implies complete oxidation of SO₂ over the 5 h.

every 0.5–1.5 mole of SO₂ oxidized, depending on whether oxidation by (R2) is followed by (R1). The sulfate-NO₂ slope in Fig. 3 is only -0.2 mol mol⁻¹, which could suggest additional NO₂ sinks associated with fog, an underestimate of sulfate in the Stage II observations as previously discussed, or a dominance of atmospheric mixing in determining the slope.

Discussion

Figure 4a illustrates our proposed mechanism for sulfate formation involving reactions (R1) and (R2) in nighttime fog and cloud associated with winter haze events. We conducted air parcel model calculations to study the pH dependence of sulfate formation in this mechanism. For reaction (R1) we used the rate expression from Martin et al.²⁸, because the much slower rate expression of Oblath et al.²⁷ would not explain the observed N₂O enhancement. For reaction (R2) we followed the rate constant (*k*₂) estimates of Lee and Schwartz⁴⁵ as 1.4 × 10⁵ M⁻¹ s⁻¹ for pH < 5 and 2 × 10⁶ M⁻¹ s⁻¹ for pH > 6, with linear interpolation between these two pH ranges. Henry's law and acid dissociation equilibrium constants for SO₂, NO₂, and HONO are in Supplementary Table 1. The air parcel was initialized with concentrations taken from the field observations during Stage I including [SO₂] = 20 ppb, [NO₂] = 80 ppb, [HONO] = 5 ppb, and then allowed to evolve as a closed system for 5 h in a nighttime fog with LWC = 0.15 g m⁻³ and T = 271 K. The time scale for equilibration between the gas and aqueous phases in fog is less than a few minutes⁴⁷, so that Henry's law can be applied to all three gases. In the case of HONO, N(III) has a lifetime against oxidation of S(IV) of 1.5 h for 20 ppb SO₂ and pH = 5.7, and this lifetime becomes longer as SO₂ is depleted.

As shown in Fig. 4b, we find in this air parcel model that reactions (R1) and (R2) are sufficiently fast for complete conversion of SO₂ to sulfate at pH > 5.5, with a maximum contribution from reaction (R1) at pH 5.5. At higher pH, the faster kinetics of reaction (R2) decrease the role of reaction (R1) in competing for SO₂ oxidation, resulting in a lower yield of N₂O. The N₂O yield would also be low (<2 ppb) if we used the faster kinetics for (R2) from Clifton et al.⁴⁶. The observed N₂O enhancement of ≈5 ppb is most consistent with the kinetics of Lee and Schwartz⁴⁵ for (R2) and Martin et al.²⁸ for (R1), with a fog/cloud pH of 5.5 (Fig. 4b), but uncertainties are obviously large. Further analysis will require better kinetic information for reactions (R1) and (R2). Decreasing ammonia emissions to bring cloud pH below 5 would shut down the mechanism (Fig. 4b), but

other SO₂ oxidation pathways may then take over such as TMI-catalyzed autoxidation²².

The role of (R2) + (R1) as a source of HONO and N₂O is of interest, considering that HONO photolysis is a major source of radicals during winter haze⁴⁸ and that N₂O is a major anthropogenic greenhouse gas. Previous studies have found that HONO in Beijing haze has a large source from direct vehicular emissions^{48,49} and this could explain the rise of HONO observed during Stage I (Fig. 1). However, the doubling of HONO concentrations from Stage I to Stage II suggests that (R2) could be an important source of HONO during haze events. With regard to N₂O, the most relevant comparison is to the national anthropogenic source for China, estimated to be 2141 Gg a⁻¹ with a dominant contribution from agriculture⁵⁰. For a rough estimate, let us assume that (R2) + (R1) is the dominant SO₂ sink during high-RH winter haze, accounting for ~8% of winter days (data downloaded from <https://rp5.ru/>), and that the N₂O molar yield is 20% based on the upper limit (pH 5.5) of Fig. 4b. The Multi-resolution Emission Inventory for China estimates a national SO₂ emission of 13.4 Tg a⁻¹ in 2016⁵¹, which would then imply a corresponding N₂O source of 36.8 Gg a⁻¹. This is small compared with the national inventory total, but not negligible as a component of N₂O emission from the energy sector estimated to be 232.7 Gg a⁻¹ in 2012⁵⁰.

In summary, we have shown from field observations of an extended winter haze PM_{2.5} pollution event in Beijing that aqueous-phase oxidation of SO₂ by NO₂ and HONO in nighttime fog and low cloud provides a plausible mechanism for explaining the rapid production of sulfate PM_{2.5}. Production of sulfate in fog and cloud is consistent with the observed shift in the sulfate size distribution to larger sizes. High-RH conditions with widespread fog and low cloud formation are typical of severe winter haze events in Beijing^{2,26}. This provides high LWCs for aqueous-phase reactions to occur, together with high pH (>5.5) from efficient uptake of ammonia. Based on available aqueous-phase kinetic data, such high-LWC high-pH conditions should allow fast oxidation of SO₂ by NO₂ to produce HONO, and subsequent fast oxidation of SO₂ by HONO to produce N₂O. There remains large uncertainty in these kinetic data. But such a mechanism is consistent with our field observations of N₂O enhancement, HONO enhancement, NO₂ depletion, and near-complete SO₂ depletion concurrent with fast sulfate production as RH increased during the haze event. Further work should target better understanding of the laboratory kinetics and products of the aqueous-phase reactions of SO₂ with NO₂ and HONO.

Methods

Field campaign. The field campaign was conducted at the Tower Site of the IAP, Chinese Academy of Science (39°58'N, 116°22'E) in Beijing, China from 4 to 22 December of 2016. This site is located around the 3rd ring road of north Beijing, surrounded by residential infrastructure and an arterial road to the east (360 m). Measurements were made from a rooftop laboratory 8 m above ground and with no interference from neighboring buildings. All data presented in this paper were hourly averaged (local time, UTC+8).

A HR-AMS was deployed during the field campaign to obtain chemical composition and size distributions of non-refractory particulate matter smaller than 1- μm diameter (NR-PM₁). A shared PM_{2.5} cyclone inlet (Model URG-2000-30ED) and a diffusion dryer were used prior to the sampling. Detailed information on the operation of HR-AMS during the sampling campaign can be found in previous literature^{4,52}. Additional measurements of aerosol composition were made with a URG-9000D Ambient Ion Monitor for water-soluble ions including a BGI-VSCC PM_{2.5} cyclone upstream. Anion analysis was performed using the IonPac AS19 hydroxide-selective anion-exchange column, which can effectively separate sulfate from HMS.

PM_{2.5} mass concentration was measured by a TDMS-TEOM PM_{2.5} analyzer (Thermo Fisher Scientific, Model 1405) at the Beijing Olympic Center Observatory, which is 4 km to the northeast of the sampling site. Fog LWC was measured by a TP/W VP-3000 ground-based 12-channel microwave radiometer (Radiometrics Corp.) at the Beijing Observatory of the China Meteorological Administration (CMA), 20 km to the south of our sampling site.

Gaseous and meteorological data were also collected at the site. An Aerodyne high-resolution time-of-flight chemical ionization mass spectrometer measured HONO concentrations⁵³. N₂O concentration was measured with a real-time CH₄/N₂O Analyzer (Los Gatos Research, Inc.). Concentrations of O₃, SO₂ (precision 0.5 ppb), and NO₂ were measured with Thermo Fisher Scientific instruments (Models 49i, 43i, 42C), and NH₃ by a Los Gatos Research analyzer. Vertical profiles of meteorological parameters, including wind speed and direction, temperature, and RH were measured from the IAP 325-m meteorological tower.

Figure 1 shows the time series of fog LWC measured at the Beijing CMA Observatory, 20 km to the south of our IAP sampling site. No fog was observed at the Observatory during Stage I (December 16–19) but pervasive nighttime fog was observed during Stage II (December 20–21) with a mean LWC of 0.15 g m⁻³ and maximum of 0.4 g m⁻³. CMA forecasts advised for strong fog (visibility 50–200 m) and extra-strong fog (visibility <50 m) across the North China Plain during the Stage II period (http://products.weather.com.cn/product/Index/index/procode/YB_W_24.shtml).

Previous studies have reported fog LWCs of 0.2–0.3 g m⁻³ in the North China Plain in association with winter haze events^{54,55}.

Calculation of fog/cloud pH. We estimated fog/cloud pH values during Stage II by assuming a pre-fog atmosphere with the mean composition observed at the IAP field site, and adding to that atmosphere an LWC of 0.15 g m⁻³. The IAP field site did not experience fog during Stage II, but cooling of a few degrees would have caused fog to form (as apparent in the low clouds observed 50 m above the site, Supplementary Fig. 2) and drive partitioning of gases into the aqueous phase. We can then estimate the fog/cloud pH from the partitioning of the relevant chemicals initially present in pre-fog air as defined by the mean conditions of Stage II (Fig. 1). This includes 14 ppb NH₃, 2 ppb SO₂, and PM_{2.5} with electroneutral composition [SO₄²⁻] = 3 × 10⁻³ mol L⁻¹, [NO₃⁻] = 6 × 10⁻³ mol L⁻¹, [Cl⁻] = 1 × 10⁻³ mol L⁻¹, and [NH₄⁺] = 1.3 × 10⁻² mol L⁻¹. We also include 400 ppm CO₂, and neglect organic acids which are low under winter haze conditions⁵⁶. Alkaline dust would increase the pH and is found to be important in precipitation data for winter Beijing^{4,57} but our mean Stage II PM_{2.5} measurements show [Ca²⁺] = 1.2 × 10⁻⁵ mol L⁻¹ and [Mg²⁺] = 2.1 × 10⁻⁵ mol L⁻¹ for the principal crustal cations, negligible relative to [NH₄⁺]. Thus we ignore the contribution of dust in the pH calculation, acknowledging that this may cause an underestimate of pH since dust could be present in larger particle sizes. We performed the pH calculation for a temperature of 271 K with the Henry's law and acid dissociation constants in Supplementary Table 1. We obtain in this manner a fog/cloud pH of 5.7.

Data availability

Datasets including time series of species concentrations and meteorological variables during the campaign are available at <https://doi.org/10.7910/DVN/FS7746>.

Received: 2 December 2019; Accepted: 14 May 2020;

Published online: 05 June 2020

References

- Sun, J. et al. Investigating the PM_{2.5} mass concentration growth processes during 2013–2016 in Beijing and Shanghai. *Chemosphere* **221**, 452–463 (2019).
- Pendergrass, D. C., Shen, L., Jacob, D. J. & Mickley, L. J. Predicting the impact of climate change on severe wintertime particulate pollution events in Beijing using extreme value theory. *Geophys. Res. Lett.* **46**, 1824–1830 (2019).
- Shen, L., Jacob, D. J., Mickley, L. J., Wang, Y. & Zhang, Q. Insignificant effect of climate change on winter haze pollution in Beijing. *Atmos. Chem. Phys.* **18**, 17489–17496 (2018).
- Zhao, J. et al. Organic aerosol processing during winter severe haze episodes in Beijing. *J. Geophys. Res. Atmos.* **124**, 10248–10263 (2019).
- Huang, R. J. et al. Contrasting sources and processes of particulate species in haze days with low and high relative humidity in winter time Beijing. *Atmos. Chem. Phys. Discuss.* **2020**, 1–29 (2020).
- Liu, Y. et al. High-time-resolution source apportionment of PM_{2.5} in Beijing with multiple models. *Atmos. Chem. Phys.* **19**, 6595–6609 (2019).
- Xue, J. et al. Sulfate formation enhanced by a cocktail of high NO_x, SO₂, particulate matter, and droplet pH during haze-fog events in megacities in China: an observation-based modeling investigation. *Environ. Sci. Technol.* **50**, 7325–7334 (2016).
- Tian, J. et al. Primary PM_{2.5} and trace gas emissions from residential coal combustion: assessing semi-coke briquette for emission reduction in the Beijing-Tianjin-Hebei region, China. *Atmos. Environ.* **191**, 378–386 (2018).
- Cheng, Y. et al. Reactive nitrogen chemistry in aerosol water as a source of sulfate during haze events in China. *Sci. Adv.* **2**, e1601530 (2016).
- Liu, T., Clegg, S. L. & Abbatt, J. P. D. Fast oxidation of sulfur dioxide by hydrogen peroxide in deliquesced aerosol particles. *Proc. Natl Acad. Sci. USA.* **117**, 1354–1359 (2020).
- Wang, G. et al. Persistent sulfate formation from London Fog to Chinese haze. *Proc. Natl Acad. Sci. USA.* **113**, 13630–13635 (2016).
- Gen, M., Zhang, R., Huang, D. D., Li, Y. & Chan, C. K. Heterogeneous SO₂ oxidation in sulfate formation by photolysis of particulate nitrate. *Environ. Sci. Technol. Lett.* **6**, 86–91 (2019).
- Xue, J. et al. Efficient control of atmospheric sulfate production based on three formation regimes. *Nat. Geosci.* **12**, 977–982 (2019).
- Seinfeld, J. H. & Pandis, S. N. *Atmospheric chemistry and physics: from air pollution to climate change*, 3rd edn, (Wiley, New York, USA, 2016).
- Wang, Y. et al. Enhanced sulfate formation during China's severe winter haze episode in January 2013 missing from current models. *J. Geophys. Res. Atmos.* **119**, 10425–10400 (2014).
- Huang, X. et al. Pathways of sulfate enhancement by natural and anthropogenic mineral aerosols in China. *J. Geophys. Res. Atmos.* **119**, 165–114, 179 (2014).
- Pandis, S. N. & Seinfeld, J. H. Mathematical modeling of acid deposition due to radiation fog. *J. Geophys. Res. Atmos.* **94**, 12911–12923 (1989).
- Pye, H. O. T. et al. The acidity of atmospheric particles and clouds. *Atmos. Chem. Phys.* **20**, 4809–4888 (2020).
- Song, S. et al. Fine particle pH for Beijing winter haze as inferred from different thermodynamic equilibrium models. *Atmos. Chem. Phys.* **18**, 7423–7438 (2018).
- Guo, H., Weber, R. J. & Nenes, A. High levels of ammonia do not raise fine particle pH sufficiently to yield nitrogen oxide-dominated sulfate production. *Sci. Rep.* **7**, 12109 (2017).
- Shi, G. et al. pH of aerosols in a polluted atmosphere: source contributions to highly acidic aerosol. *Environ. Sci. Technol.* **51**, 4289–4296 (2017).
- Shao, J. et al. Heterogeneous sulfate aerosol formation mechanisms during wintertime Chinese haze events: air quality model assessment using observations of sulfate oxygen isotopes in Beijing. *Atmos. Chem. Phys.* **19**, 6107–6123 (2019).
- Li, J. et al. Stable sulfur isotopes revealed a major role of transition-metal-ion catalyzed SO₂ oxidation in haze episodes. *Environ. Sci. Technol.* **54**, 2626–2634 (2020).
- Jacob, D. J. Heterogeneous chemistry and tropospheric ozone. *Atmos. Environ.* **34**, 2131–2159 (2000).
- Song, S. et al. Possible heterogeneous chemistry of hydroxymethanesulfonate (HMS) in northern China winter haze. *Atmos. Chem. Phys.* **19**, 1357–1371 (2019).
- Moch, J. M. et al. Contribution of hydroxymethane sulfonate to ambient particulate matter: a potential explanation for high particulate sulfur during severe winter haze in Beijing. *Geophys. Res. Lett.* **45**, 11969–11979 (2018).
- Oblath, S. B., Markowitz, S. S., Novakov, T. & Chang, S. G. Kinetics of the initial reaction of nitrite ion in bisulfite solutions. *J. Phys. Chem.* **86**, 4853–4857 (1982).
- Martin, L. R., Damschen, D. E. & Judeikis, H. S. The reactions of nitrogen oxides with SO₂ in aqueous aerosols. *Atmos. Environ.* **15**, 191–195 (1981).
- Chang, S. G., Toossi, R. & Novakov, T. The importance of soot particles and nitrous acid in oxidizing SO₂ in atmospheric aqueous droplets. *Atmos. Environ.* **15**, 1287–1292 (1981).
- Jayne, J. T. et al. Development of an aerosol mass spectrometer for size and composition analysis of submicron particles. *Aerosol Sci. Technol.* **33**, 49–70 (2000).

31. Tian, H. et al. Global methane and nitrous oxide emissions from terrestrial ecosystems due to multiple environmental changes. *Ecosys. Heal. Sustain* **1**, 1–20 (2015).
32. Wallington, T. J. & Wiesen, P. N₂O emissions from global transportation. *Atmos. Environ.* **94**, 258–263 (2014).
33. Park, J. Y. & Lee, Y. N. Solubility and decomposition kinetics of nitrous acid in aqueous solution. *J. Phys. Chem.* **92**, 6294–6302 (1988).
34. McKeen, S. A. et al. Hydrocarbon ratios during PEM-WEST A: a model perspective. *J. Geophys. Res. Atmos.* **101**, 2087–2109 (1996).
35. Brasseur, G. P. & Jacob, D. J. Modeling of atmospheric chemistry. (Cambridge University Press, 2017).
36. Xu, W. et al. NH₃-promoted hydrolysis of NO₂ induces explosive growth in HONO. *Atmos. Chem. Phys.* **19**, 10557–10570 (2019).
37. Pan, Y. et al. Fossil fuel combustion-related emissions dominate atmospheric ammonia sources during severe haze episodes: evidence from ¹⁵N-stable isotope in size-resolved aerosol ammonium. *Environ. Sci. Technol.* **50**, 8049–8056 (2016).
38. Weber, R. J., Guo, H., Russell, A. G. & Nenes, A. High aerosol acidity despite declining atmospheric sulfate concentrations over the past 15 years. *Nat. Geosci.* **9**, 282–285 (2016).
39. Wang, G. et al. Particle acidity and sulfate production during severe haze events in China cannot be reliably inferred by assuming a mixture of inorganic salts. *Atmos. Chem. Phys.* **18**, 10123–10132 (2018).
40. Liu, M. et al. Fine particle pH during severe haze episodes in northern China. *Geophys. Res. Lett.* **44**, 5213–5221 (2017).
41. Jacob, D. J., Waldman, J. M., Munger, J. W. & Hoffmann, M. R. The H₂SO₄-HNO₃-NH₃ system at high humidities and in fogs: 2. Comparison of field data with thermodynamic calculations. *J. Geophys. Res. Atmos.* **91**, 1089–1096 (1986).
42. Shi, G. et al. Aerosol pH dynamics during haze periods in an urban environment in China: use of detailed, hourly, speciated observations to study the role of ammonia availability and secondary aerosol formation and urban environment. *J. Geophys. Res. Atmos.* **124**, 9730–9742 (2019).
43. Xie, Y. et al. Enhanced sulfate formation by nitrogen dioxide: Implications from in situ observations at the SORPES station. *J. Geophys. Res. Atmos.* **120**, 12679–12694 (2015).
44. Xue, J., Yuan, Z., Yu, J. Z. & Lau, A. K. H. An observation-based model for secondary inorganic aerosols. *Aerosol Air Qual. Res.* **14**, 862–878 (2014).
45. Lee, Y. N., & Schwartz, S. E. Kinetic of oxidation of quueous sulfur(IV) by nitrogen dioxide. In precipitation Scavenging, Dry Deposition and Resuspension. **1** (eds Pruppacher, H. R. et al.), (Elsevier, New York, USA, 1983).
46. Clifton, C. L., Altstein, N. & Huie, R. E. Rate constant for the reaction of nitrogen dioxide with sulfur(IV) over the pH range 5.3–13. *Environ. Sci. Technol.* **22**, 586–589 (1988).
47. Jacob, D. J. Comment on “The photochemistry of a remote stratiform cloud” by William L. Chameides. *J. Geophys. Res. Atmos.* **90**, 5864–5864 (1985).
48. Liu, Y. et al. The promotion effect of nitrous acid on aerosol formation in wintertime Beijing: possible contribution of traffic-related emission. *Atmos. Chem. Phys. Discuss.* **2020**, 1–43 (2020).
49. Zhang, W. et al. Variations and sources of nitrous acid (HONO) during a severe pollution episode in Beijing in winter 2016. *Sci. Total. Environ.* **648**, 253–262 (2019).
50. Zhang, B., Zhang, Y., Zhao, X. & Meng, J. Non-CO₂ greenhouse gas emissions in China 2012: inventory and supply chain analysis. *Earths Future* **6**, 103–116 (2018).
51. Zheng, B. et al. Trends in China’s anthropogenic emissions since 2010 as the consequence of clean air actions. *Atmos. Chem. Phys.* **18**, 14095–14111 (2018).
52. Wang, J. et al. Characterization of black carbon-containing fine particles in Beijing during wintertime. *Atmos. Chem. Phys.* **19**, 447–458 (2019).
53. Zhou, W. et al. Production of N₂O₅ and ClNO₂ in summer in urban Beijing, China. *Atmos. Chem. Phys.* **18**, 11581–11597 (2018).
54. Deng, C., Yin, X. & Gan, L. Stratification characteristic analysis of atmospheric liquid water content and relative humidity during fog and haze weather in Beijing. *Clim. Environ. Res.* **19**, 193–199 (2014).
55. Quan, J. et al. Analysis of the formation of fog and haze in North China Plain (NCP). *Atmos. Chem. Phys.* **11**, 8205–8214 (2011).
56. Yu, Q. et al. Characteristics and secondary formation of water-soluble organic acids in PM₁, PM_{2.5} and PM₁₀ in Beijing during haze episodes. *Sci. Total Environ.* **669**, 175–184 (2019).
57. Turpin, B. J. & Lim, H.-J. Species contributions to PM_{2.5} mass concentrations: revisiting common assumptions for estimating organic mass. *Aerosol Sci. Technol.* **35**, 602–610 (2001).

Acknowledgements

This work is a contribution from the Harvard-NUIST Joint Laboratory for Air Quality and Climate (JLAQC). We acknowledge support from the Samsung Advanced Institute of Technology, the National Natural Science Foundation of China (Grant No. 91544220, 21777073, 91744207, 21577063, 21577065, and 41875167), and the National Key Research and Development Program of China (2018YFC0213802). J. L. acknowledges support from the Startup Fund for Talent at NUIST. We thank Loretta Mickley and Jonathan Moch (Harvard) for helpful comments.

Author contributions

J.W., J.L., X.G., Y.L.S. and M.C. designed the research; J.W., J.Y., X.G. and D.J.J. led the writing; J.W., J.Z., Y.W., D.N., F.S., X.H., D.J., X.S., J.G., H.L., D.D.H., and D.L. performed experiments; J.W., J.Y., X.G., and D.J.J. analyzed the data; J.W., J.Y., J.L., and D.J.J. performed NO₂ and HONO mechanism analysis and the air parcel model simulation; J.H., W.X., S.S., Y.Q., P.L., J.R.T., H.C.L., S.H., S.T.M., and Q.Z. contributed significant comments and editing of the paper.

Competing interests

The authors declare no competing interests.

Additional information

Supplementary information is available for this paper at <https://doi.org/10.1038/s41467-020-16683-x>.

Correspondence and requests for materials should be addressed to X.G. or D.J.J.

Peer review information *Nature Communications* thanks Yafang Cheng and the other, anonymous, reviewer(s) for their contribution to the peer review of this work. Peer reviewer reports are available.

Reprints and permission information is available at <http://www.nature.com/reprints>

Publisher’s note Springer Nature remains neutral with regard to jurisdictional claims in published maps and institutional affiliations.



Open Access This article is licensed under a Creative Commons Attribution 4.0 International License, which permits use, sharing, adaptation, distribution and reproduction in any medium or format, as long as you give appropriate credit to the original author(s) and the source, provide a link to the Creative Commons license, and indicate if changes were made. The images or other third party material in this article are included in the article’s Creative Commons license, unless indicated otherwise in a credit line to the material. If material is not included in the article’s Creative Commons license and your intended use is not permitted by statutory regulation or exceeds the permitted use, you will need to obtain permission directly from the copyright holder. To view a copy of this license, visit <http://creativecommons.org/licenses/by/4.0/>.

© The Author(s) 2020